Available online at www.sciencedirect.com

ScienceDirect

Procedia Structural Integrity 21 (2019) 91–100

Structural Integrity Procedia

www.elsevier.com/locate/procedia

1st International Workshop on Plasticity, Damage and Fracture of Engineering Materials

Finite Element Modelling of TBC Failure Mechanisms by Using XFEM and CZM

Safa Mesut Bostancı[a,b,*], Ercan Gürses[a], Demirkan Çöker[a]

[a] *Aerospace Engineering Dept. METU, Ankara 06800, Turkey*
[b] *ASELSAN INC., Macunköy, Ankara 06370, Turkey*

Abstract

Thermal Barrier Coatings have been widely used in modern turbine engines to protect the nickel based metal substrate from the high temperature service conditions, 1600-1800 K. In this study, failure mechanisms of typical Air Plasma Sprayed Thermal Barrier Coatings (TBC) used in after-burner structures composed of three major layers: Inconel 718 substrate, NiCrAlY based metallic bond coat (BC) and Yttria Stabilized Zirconia (YSZ) based ceramic top coat (TC) are investigated. Investigation of the cracking mechanism of TBC in terms of design and performance is very important because the behavior of TBCs on ductile metallic substrates is brittle. To this end, four-point bending experiments reported in Kütükoğlu (2015) are analyzed by using the Extended Finite Element Method (XFEM) and the Cohesive Zone Method (CZM). All the analyses are conducted with the commercial finite element software ABAQUS. Three different models with varying TC and BC thicknesses are studied. It is observed that multiple vertical cracks are initiated in the TC. Cracks initiate at the top of YSZ and propagate through the whole TC until they reach the interface between the TC and the BC. Then, delaminations at the interface between the TC and the BC start. It is observed that the average spacing of cracks in TC increases with the increasing thickness of the TC and the delamination becomes prominent with the increasing TC thickness. Numerical results are found to be consistent with the experimental results.

Keywords: eXtended Finite Element Method; Cohesive Zone Method; Thermal Barrier Coatings;

1. Introduction

From past to present, in recent decades, many studies have been conducted to find answers to increase the efficiency of gas turbines. To this end, insulation or cooling of the hot section components such as vanes and blades of an advanced turbine or an engine in modern aerospace applications is one of the main

* Corresponding author. Tel.: +90-507-702-1551.
E-mail address: smbostanci@aselsan.com.tr

10.1016/j.prostr.2019.12.090

problems. At this point, thermal barrier coating systems (TBCs) are of a great interest for many researchers since application of these coatings under optimum conditions enables many components to operate at higher gas temperatures Clarke et al. (2005).

Contemporary applications show that there are two main methods to apply TBC coatings known as air plasma spraying (APS) and electron beam physical vapor deposition (EB-PVD). The APS method that is used to coat stationary engine parts is a considerably cheaper method than the EB-PVD whereas the EB-PVD is mostly used to coat the hot sections of the jet engines such as blades and vanes. Current applications for both stationary and rotating sections faced with hot temperatures are coated by the APS method.

The air plasma spraying, in other words, atmospheric plasma spraying is basically a thermal spraying method consisting of composition of the cladding environment, i.e., the plasma steam and the powder material, to be deposited on the substrate material in order to provide thermal, wear and corrosion resistance.

In general, a superalloy/TBC system consists of plasma sprayed ZrO_2-Y_2O_3, in other words, Yttria Stabilized Zirconia (YSZ) ceramic layer and a NiCrAlY bond coat on a substrate made of nickel based superalloy Swadyba et al. (2007). In this study, the cracking mechanism of an APS TBC under four point bending is investigated by using an approach that combines the XFEM and the CZM.

2. Method

2.1. Extended Finite Element Method

The XFEM has been used to investigate crack initiation and growth behaviour of different engineering materials in recent years. Furthermore, it became one of the most popular computational tools to study many crack problems because in general it allows initiation of multiple cracks, does not require any initial crack and remeshing. The XFEM is based on the partition of unity concept.

2.1.1. Partition of Unity Finite Element Method

The accuracy of a finite element solution can be improved by using so-called enrichment procedure. In other words, if an a priori known analytical solution of the problem is included to the finite element formulation the accuracy of results can be increased. The number of the nodal degrees of freedom increase as this concept is adapted to fracture mechanics problems because the analytical crack-tip solution is incorporated to the framework of the isoparametric finite element discretization to improve the crack-tip field prediction, see Mohammadi (2008).

The partition of unity property is satisfied by the set of isoparametric finite element shape functions N_j

$$\sum_{j=1}^{m} N_j(x) = 1 \tag{1}$$

The partition of unity finite element method (PUFEM), proposed by Melenk (1996), uses the concept of enrichment functions in conjunction with the partition of unity property given in (1). PUFEM, as given (2) provides the approximation of the displacement within an element by using $p_i(x)$ and a_{ji} which are the enrichment functions and the additional degrees of freedom related to the enriched solution respectively.

$$u^h(x) = \sum_{j=1}^{m} N_j(x) \left(u_j + \sum_{i=1}^{n} p_i(x) a_{ji} \right) \tag{2}$$

The total number of nodes of each element is determined by m and the number of enrichment functions p_i is determined by n. (2) can be written for an enriched node x_k

$$u^h(x_k) = \left(u_k + \sum_{i=1}^{n} p_i(x_k) a_{ji} \right). \tag{3}$$

However, (3) does not satisfy the interpolation property at node k. Therefore, the enriched displacement field is modified as follows to get around this problem

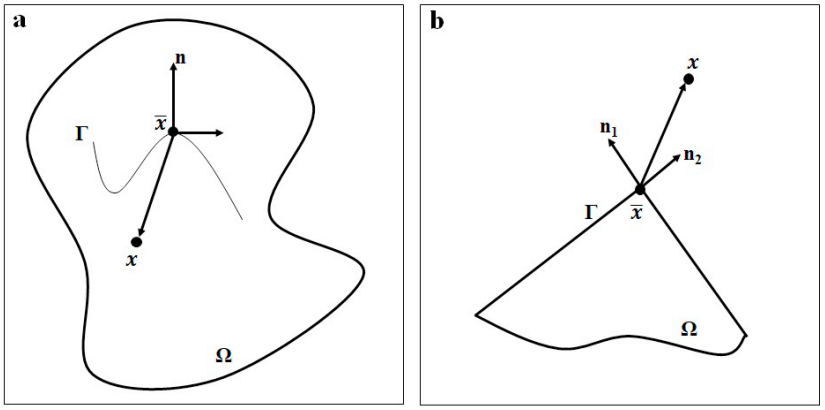

Fig. 1: (a) smooth crack (b) kinked crack

$$u^h(x) = \sum_{j=1}^{m} N_j(x) \left[u_j + \sum_{i=1}^{n} (p_i(x) - p_i(x_j)) a_{ji} \right]. \tag{4}$$

2.1.2. Generalized Finite Element Method

In generalized finite element method (GFEM), see Strouboulis et al. (2001), shape functions are used for the ordinary and enriched parts of the finite element discretization independently to increase the order of integrity, i.e.

$$u^h(x) = \sum_{j=1}^{m} N_j(x) u_j + \sum_{j=1}^{m} \overline{N}_j(x) \left(\sum_{i=1}^{n} p_i(x) a_{ji} \right) \tag{5}$$

where $\overline{N}_j(x)$ are the shape functions related to enrichment basis functions $p_i(x)$. However, the interpolation at nodal points are not satisfied in (5) as well. Therefore, the same procedure explained in previous section is applied to get around this problem

$$u^h(x) = \sum_{j=1}^{m} N_j(x) u_j + \sum_{j=1}^{m} \overline{N}_j(x) \left[\sum_{i=1}^{n} (p_i(x) - p_i(x_j)) a_{ji} \right]. \tag{6}$$

2.1.3. Enrichment Functions

In two-dimensional problems, cracks are modelled by means of two different types of enrichment functions.

- **Heaviside Enrichment Function**

$$H(x,y) = \begin{cases} 1 & \textbf{for} \quad (x - \overline{x}) \cdot \mathbf{n} > \mathbf{0} \\ -1 & \textbf{for} \quad (x - \overline{x}) \cdot \mathbf{n} < \mathbf{0} \end{cases} \tag{7}$$

For Heaviside enrichments, only the nodes that belong to an element split by a discontinuity may be used. The Heaviside function is able to model a jump in the displacement field which is caused by the splitting of the domain by a crack. In a deformable body Ω in Fig. 1, the continuous curve Γ represents a crack in the domain, and $\mathbf{x}(x,y)$ is an arbitrary point in the body, $\overline{\mathbf{x}}(x,y)$ is the closest point to $\mathbf{x}(x,y)$ that belongs to Γ and $\mathbf{n}$ is the outward normal vector of the Γ at point $\overline{\mathbf{x}}(x,y)$. The

Heaviside function can be defined as in (7) to determine the position of $\mathbf{x}(x,y)$ with respect to the crack location. The Heaviside function introduces the discontinuity across the crack faces.

- **Asymptotic Near-Tip Field Function**
The Heaviside function could not be used to approximate the displacement field in the entire element which are not completely damaged, in other words elements that contain the crack tip. Instead asymptotic near-tip field enrichment functions originally introduced by Fleming et al. (1997) can be used for the use in Element-Free Galerkin method (EFG). These functions have been extensively used for fracture problems and later they were employed by Belytschko and Black (1999) in XFEM formulation. Following four functions expressed in local crack tip polar coordinate system (r,θ) are responsible to define the fracture tip displacement field

$$\{F_i(r,\theta)\}_{i=1}^{4} = \left\{ \sqrt{r}\cos(\frac{\theta}{2}),\ \sqrt{r}\sin(\frac{\theta}{2}),\ \sqrt{r}\sin(\frac{\theta}{2})\sin(\theta),\ \sqrt{r}\cos(\frac{\theta}{2})\sin(\theta) \right\}. \tag{8}$$

By using four enrichment functions in (8) new degrees of freedom are included at each node in every direction. The term $\sqrt{r}\sin(\theta/2)$ defines the discontinuity in the approximation over the crack tip because it is the only discontinuous function through the crack surface. However, other three functions are used in the neighbourhood of the crack tip only to improve the solution of the finite element approximation, especially improve the accuracy of the calculation of stress intensity factors, see Moës et al. (1999).
Following expression could be used based on the four enrichment functions given in (8)

$$\begin{aligned} u^h(x) = u_{FEM}(x) + u_{ENR}(x) = \sum_{i\in I} N_i(x)u_i + \sum_{j\in J} N_j[H(x)]a_j \\ + \sum_{k\in K_1} N_k(x)\left[\sum_{l=1}^{4} b_k^{l_1} F_l^1(x)\right] + \sum_{k\in K_2} N_k(x)\left[\sum_{l=1}^{4} b_k^{l_2} F_l^2(x)\right] \end{aligned} \tag{9}$$

Furthermore, (9) can be reformulated to satisfy interpolation property as follows

$$\begin{aligned} u^h(x) = \sum_{i\in I} N_i(x)u_i + \sum_{j\in J} N_j\left[H(x) - H(x_j)\right]a_j + \sum_{k\in K_1} N_k(x)\left[\sum_{l=1}^{4} b_k^{l_1}\left[F_l^1(x) - F_l^1(x_k)\right]\right] \\ + \sum_{k\in K_2} N_k(x)\left[\sum_{l=1}^{4} b_k^{l_2}\left[F_l^2(x) - F_l^2(x_k)\right]\right] \end{aligned} \tag{10}$$

where J represents set of nodes of the elements which are splitted by the crack completely and as explained previously enriched with the Heaviside enrichment function. K_1 and K_2 are the sets of nodes whose support domains include fracture tips 1 and 2, and their near tip enrichment functions are $F_l^1(x)$ and $F_l^2(x)$, respectively. $b_k^{l_1}$ and $b_k^{l_2}$ are the vectors of additional degrees of freedom used to model fracture tips. u_i indicates the conventional degrees of freedom and a_j describes the additional degrees of freedom used to model crack faces.

2.1.4. Traction-Separation Law

The linear traction-seperation law proposed by Alfano and Crisfield (2001) as shown in Fig. 2a is used for the XFEM enriched region in TC. In Fig. 2a, the horizontal axis of the graph refers to the separation and the vertical axis is the traction. The slope of the initial part k is the cohesive stiffness. The damage initiation occurs at point X, therefore k gives the value of the cohesive stiffness which is the ratio of traction stress to separation at point X. At point Y, an unloading occurs and the cohesive stiffness decreases to $(1-D)k$ for the next time increment. D is the damage parameter and it is defined by user and the value of D is zero before damage initiation. The damage initiation occurs at point X and it finishes at point Z. The values of

D are 0 and 1, respectively at points X and Z. In Fig. 2b derivation of damage parameter D is shown. The loading stiffness $m = (1 - D)k$ derived as in (11) from Fig. 2

$$m = (1 - D)\left(\frac{T^u}{\delta_y}\right) \tag{11}$$

$T^u/(\delta_y)$ gives the undamaged crack stiffness value k. T^u is the stress when there is no cohesive damage and T^d is the actual traction stress with cohesive damage. Then the following condition can be derived from Fig. 2

$$T^u \frac{(\delta_z - \delta_y)}{(\delta_z - \underline{\delta})} = \delta_y(1 - D)\left(\frac{T^u}{\delta_y}\right) \tag{12}$$

The damage parameter D can be written in terms of seperation (δ), by simplifying (12) as

$$D = \frac{\delta_z(\delta_y - \underline{\delta})}{\delta_y(\delta_z - \underline{\delta})} \tag{13}$$

When the energy release rate due to the crack opening exceeds the critical energy release rate (G_C) the ultimate failure occurs. G_C can be calculated by the area under the curve in Fig. 2. The type of failure strongly depends on the value of G_C; high and low G_C are related to the ductile and brittle failure, respectively. The critical crack opening (δ_z) depends on the fracture stress ($\underline{T}$) and the fracture toughness (K_I^C), and the relationship for mode I failure is as follows

$$\delta_z = \frac{2(K_I^C)^2}{E\underline{T}} \tag{14}$$

Detailed discussion on relations given in equations (11), (12), (13), (14) can be found in Kyaw et al. (2016).

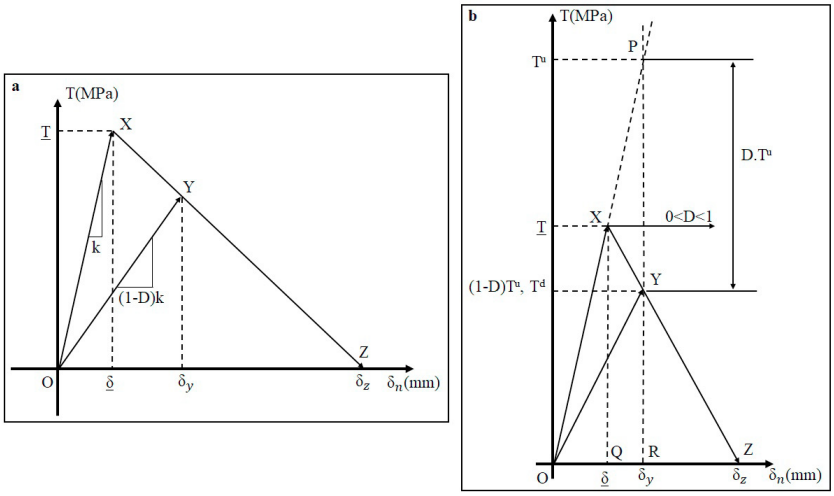

Fig. 2: (a) Linear traction-seperation law; (b) Damage parameter and unloading process

2.2. Cohesive Zone Method

The Cohesive Zone Method (CZM) has been introduced in the early sixties to analyse fracture under static loading beyond the crack tip by Barenblatt (1962). A cohesive zone law, also known as traction-separation law, describes the constitutive behaviour between the relative displacement δ between two

points and traction T as a curve, see Noorman (2014). ABAQUS allows two different methods to utilize cohesive zone method to a finite element model. These are surface based and element based cohesive behaviour. In this study, surface based cohesive behaviour is used to model delamination at the TC/BC interface.

The surface-based cohesive behavior is defined as a surface interaction property and can be used to model the delamination at interfaces directly by using a traction-seperation constitutive model. Unlike the element based cohesive behaviour, the surface-based cohesive behavior provides a simplified way to model cohesive connections with negligibly small interface thicknesses.

The damage initiation criterion given in (15) and the damage evolution law used in surface-based cohesive behavior are very similar to those used for cohesive elements with traction-separation constitutive model. A linear elastic traction-separation behavior, relates normal and shear stresses to the normal and shear separations across the interface before the initiation of any damage. The damage evolution describes the degradation of the cohesive stiffness.

The maximum stress damage initiation criterion given in (15) is used in this study.

$$MAX\left\{\frac{\langle t_n\rangle}{t_n^{max}}, \frac{t_s}{t_s^{max}}, \frac{t_t}{t_t^{max}}\right\} = 1 \tag{15}$$

In (15) t_{n} describes the normal contact stress in the pure normal mode, t_{s} describes shear contact stress along the first shear direction, t_{t} is the shear contact stress along the second shear direction, see ABAQUS User Guide (2013).

3. Finite Element Model

Two-dimensional finite element models of the symmetric four point bending experiments conducted in Kutukoglu (2015) are created. There are three different TBC specimens with different BC and TC thicknesses. The geometry and the coating thicknesses of three different specimens are given in Table 2.

Two-dimensional models are created, because three-dimensional effects are considered to be negligible for the problem. In the four point bending tests given in Fig. 3, the substrate thicknesses are same for all three models, while BC and TC thicknesses vary. The models are constrained by four circular rigid bodies, the two of them are used to support the beam and the other two are used to apply the load. The distance L between supports is 14 mm and the distance $2L$ between the loads is 28 mm respectively given in Fig. 3, and the total model length is 40 mm. Frictionless contacts are used between the rigid bodies and the specimens. The rigid body supports are constrained with encastre boundary condition and a displacement controlled loading in y-direction is applied with two rigid bodies from the TC. In this study, displacement controlled static analysis have been performed and 2 mm displacement is synchronously applied from the loading points to every model.

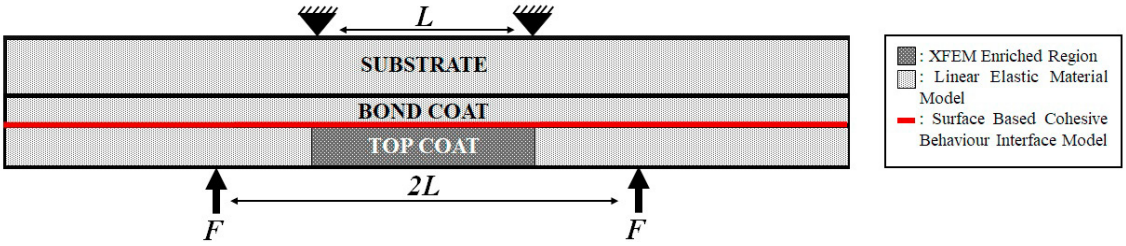

Fig. 3: Schematic view of the four point bending test

Material properties given in Table 1 are taken from the literature Kutukoglu (2015) except the Young's Modulus of the TC. The Young's Modulus of the Top Coat layer is calculated by nanoindentation test in Kutukoglu (2015) as 118 GPa with a 17 GPa standard deviation. On the other hand Qi et al. (2005) conducted

cantilever beam experiments for similar systems. Since the bending experiments for the determination of the Young's Modulus is more relevant for the problem considered in this study, the Young's modulus of 45 GPa found in Qi et al. (2005) is used.

Table 1: Material Properties

Layer	E [GPa]	Poissons Ratio	MAXPS[MPa]	$G_{critical}$[kJ/m^2]
Substrate (Inconel 718)	205	0.284	-	-
Bond Coat (NiCrAlY)	115	0.3	-	-
Top Coat (YSZ)	45	0.157	1000	8.27

The Maximum Principal Stress Criterion (MAXPS) is used as a damage initiation criterion for the failure model of the YSZ in XFEM enriched region. The parameter MAXPS is determined according to the experimental results of Kutukoglu (2015) and it is adjusted by iterations based on the crack nucleation times found in experiments. The bending tensile strength is calculated by Kondoh et al. (2004) as 1000 MPa for 3YSZ and the results of the iterative study is validated for 3YSZ. The porosity of TBC coatings is one the most important properties, see Moskal (2007). To model porosity or micro cracks in the YSZ a script is written and MAXPS value of uppermost layer elements is fluctuated around 1000 MPa by this script. The script randomly distributes MAXPS parameter in user-defined limits in the uppermost layer elements of the TC layer. Fluctuation limits set as $\pm 3.5\%$ which are also found by an iterative study in the thick specimen according to the experimental results.

Table 2: Substrate and coating thicknesses of the specimen

Specimen	Top Coat [mm]	Bond Coat [mm]	Substrate[mm]
Thick	0.6	0.16	1.6
Standard	0.38	0.1	1.6
Thin	0.26	0.05	1.6

Four node plane strain elements with reduced integration (CPE4R) used throughout the model. In the TC and the BC 0.05 mm mesh size is used. In substrate layer of the model mesh size varies through the thickness direction and increases from 0.05 mm up to 0.2 mm. The employed mesh sizes are determined by a mesh convergence study.

4. Results

The cracking mechanism of TBC is crucial for its design and performance. TBCs coated on metallic substrates show a very brittle fracture behaviour and their failures are very dependent to TC/BC interface delamination. Therefore, the failure mechanism and the failure sequence are investigated in this numerical study.

Table 3: Number of cracks for different models.

TC Thickness	Thin	Standard	Thick
Model - 1	8	8	6
Model - 2	8	7	6
Model - 3	9	8	5

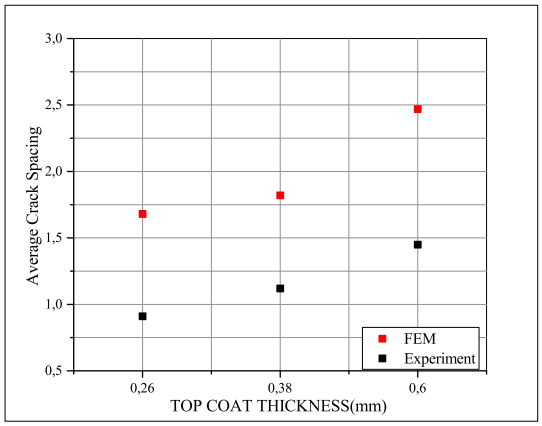

Fig. 4: Average crack spacing for different top coat thicknesses

In order to compare with experiments average crack spacing in the TC are studied. To this end three different finite element models for thin, standard and thick specimens are generated. The three FE models for each specimen have different randomly assigned MAXPS parameters in the uppermost layer finite elements in the TC. The total average crack spacing results are determined as the average of the 3 different finite element analysis results. The results are given in terms of number of cracks in Table 3 for each model and each specimen.

The average crack spacing results of the TC layer are also presented in Fig. 4 together with the experimantal results of Kutukoglu (2015). According to the results it can be seen that the change in average crack spacing with TC thickness is similar in simulations and experiments. Both the experiments and the finite element results show that the increase in thickness of TC results in an increase in average crack spacing.

Symmetrical four-point bending generates a constant moment region, thus similar maximum principal stresses occur at the uppermost layer elements between two supports. Therefore, without variation of MAXPS parameter in FEM models, cracks initiate almost simultaneously in many enriched elements at the uppermost layer of the TC.

The main purpose of the work is to investigate the cracking mechanism of TBCs and study the variation of average crack spacing with coating thickness change. The cracking mechanism of different thickness TBC specimens are similar i.e., first, cracks perpendicular to surface initiate at the uppermost layer elements and they propogate through the TC layer vertically. Then, vertical cracks reach to TC/BC interface and stop, followed by delamination initiation and propagation through the interface. Delamination is more prominent in the thick model compared to standard and thin models as it was observed in experiments of Kutukoglu (2015). In other words, simulation results of combined XFEM/CZM model show similar behaviour with the experiments of Kutukoglu (2015), see Fig. 5.

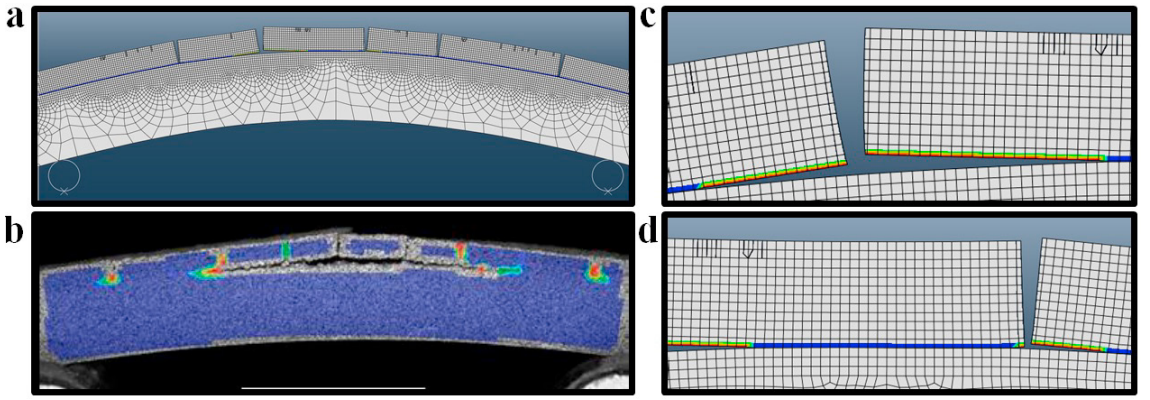

Fig. 5: Thick Model; (a) FEM results; (b) experimental results; (c) delamination TC/BC interface; (d) delamination TC/BC interface.

5. Conclusion

In this study, failure mechanisms of APS TBC are numerically investigated under four-point bending loading by using a combined XFEM/CZM model in commercial software ABAQUS. The XFEM is used to monitor the crack initiation and propogation at the TC and the CZM is used to model the delamination at the interface. One of the main purposes of this study is to investigate the failure mechanisms of the TBC by numerical methods. In simulations and experiments cracks initiate at the uppermost layer of the TC and propagate through the TC and delaminations occur at the interface after vertical cracks reach the TC/BC interface. The average crack spacing increases as the thickness of YSZ layer increases. Furthermore, delamination failure becomes more prominent as YSZ layer thickness increases.

Acknowledgements

This study is supported by ASELSAN Inc.

References

Clarke, D.R., Phillpot, S.R., 2005, "Thermal barrier coating materials", Materials Today, vol. 8, no. 6, pp. 22-29.

Kyaw, S.T., Jones, I.A. Hyde, T.H., 2016, "Simulation of failure of air plasma sprayed thermal barrier coating due to interfacial and bulk cracks using surface-based cohesive interaction and extended finite element method", Journal of Strain Analysis for Engineering Design, vol. 51, no. 2, pp. 132-143.

Belytschko, T., Black, T. 1999, "Elastic crack growth in finite elements with minimal remeshing", International Journal for Numerical Methods in Engineering, vol. 45, no. 5, pp. 601-620.

Melenk, J.M., Babuška, I. 1997, "Approximation with harmonic and generalized harmonic polynomials in the partition of unity method", Computer Assisted Mechanics and Engineering Sciences, vol. 4, no. 3-4, pp. 607-632.

Belytschko, T., Gracie, R., Ventura, G. 2009, "A review of extended/generalized finite element methods for material modeling", Modelling and Simulation in Materials Science and Engineering, vol. 17, no. 4.

Alfano, G., Crisfield, M.A. 2001, "Finite element interface models for the delamination analysis of laminated composites: Mechanical and computational issues", International Journal for Numerical Methods in Engineering, vol. 50, no. 7, pp. 1701-1736.

Qi, H.-., Zhou, L.-., Yang, X.-. 2005, "Measurement of Young's modulus and Poisson's ratio of thermal barrier coatings", Chinese Journal of Aeronautics, vol. 18, no. 2, pp. 180-184.

Mohammadi, S., 2008. Extended Finite Element Method for Fracture Analysis of Structures. 1st ed. Oxford: Blackwell Publishing Ltd.

Moskal, G., 2007. "The porosity assessment of thermal barrier coatings obtained by aps method". Journal of Achievements in Materials and Manufacturing Engineering, 20(1-2), pp. 483–486.

Kutukoglu, B., 2015. Experimental investigation of the failure of air plasma sprayed thermal barrier coatings. MSc. thesis, METU, Ankara

Noorman, D.C, 2014. Cohesive zone modelling in adhesively bonded joints. MSc. thesis, TU DELFT, Delft

Swadyba, L., Moskal, G., Mendala, B., and Gancarczyk, T., 2007. "Characterisation of aps tbc system during isothermal oxidation at 1100 c". Archives of Materials Science, 758, p.758.

Systems, D., 2013. “Abaqus 6.14–analysis users guide: Volume iv: Elements”. Providence, Rhode Island.
Strouboulis, T., Copps, K., Babuška, I. 2001, ”Computational mechanics advances. The generalized finite element method”, Computer Methods in Applied Mechanics and Engineering, vol. 190, no. 32-33, pp. 4081-4193.
Melenk, J.M., Babuška, I., 1996, ”The partition of unity finite element method: Basic theory and applications”, Computer Methods in Applied Mechanics and Engineering, vol. 139, no. 1-4, pp. 289-314.
Fleming, M., Chu, Y.A., Moran, B., Belytschko, T. 1997, ”Enriched element-free galerkin methods for crack tip fields”, International Journal for Numerical Methods in Engineering, vol. 40, no. 8, pp. 1483-1504.
Barenblatt, G.I. 1962, The Mathematical Theory of Equilibrium Cracks in Brittle Fracture.
Kondoh, J., Shiota, H., Kawachi, K., Nakatani, T. 2004, ”Yttria concentration dependence of tensile strength in yttria-stabilized zirconia”, Journal of Alloys and Compounds, vol. 365, no. 1-2, pp. 253-258.
Moës, N., Dolbow, J., Belytschko, T. 1999, ”A finite element method for crack growth without remeshing”, International Journal for Numerical Methods in Engineering, vol. 46, no. 1, pp. 131-150.